Analysis of Laser Backscattering from Solid Fuel Rocket Plumes

C. T. Christou* and D. A. Levin*
Institute for Defense Analyses, Alexandria, Virginia 22311

Analyses have been carried out for a ground-based experiment to measure laser backscattering from solid fuel rocket plumes. Mie scattering theory was used to compute the returned laser power as a function of range, wavelength, and scattering angle. The feasibility of retrieval of plume particle properties through various inversion methods was examined. The effects of atmospheric conditions on the detectability of the returned signal were also considered.

Nomenclature

A_r	= effective receiver aperture
a	= radius of particle
a_m	= radial measure defined such that 99% of the particles in a size distribution have radii smaller than a_m
a_{max}	= maximum radius in distribution
a_{min}	= minimum radius in distribution
a_{mode}	= most probable radius of a particle size distribution
c	= speed of light, 3×10^8 m/s
$(d\sigma/d\Omega)(\lambda,\theta,a)$	= differential scattering cross section
$f(a)$	= particle size distribution function
K	= efficiency of total optical system
$K(\lambda,\theta,a)$	= kernel function
$m(a)$	= mass loading distribution
N	= number density of scattering particles
$N_i(r)$	= number density of species i at distance r
P_o	= transmitted power of laser pulse
P_r	= received laser power
R	= distance from scattering volume to detector
$T(\nu_o)$, $T(\nu_r)$	= one-way transmittances at the transmitted and received frequencies
$Y(R)$	= geometrical factor to account for the overlap of transmitter and receiver fields of view
$\alpha(\nu,r)$	= total extinction coefficient by gaseous species and particulates in plume, as well as atmospheric constituents
$\beta(\nu_o,R)$	= volume backscattering coefficient in units of inverse length
$\Delta R = c\tau/2 = (c/2) \times (\tau_p + \tau_s + \tau_c)$	= range resolution of measurement
θ	= scattering angle
λ	= wavelength of laser radiation
ν_o, ν_r	= transmitted and received laser frequencies
ρ	= bulk matter density of particulate species
σ, $\sigma_i(\nu)$	= extinction cross section (of species i)
τ_c	= detection system response time
τ_p	= laser pulse length
τ_s	= species optical interaction time

Received April 2, 1990; revision received Aug. 31, 1990; second revision received Oct. 12, 1990; accepted for publication Oct. 24, 1990.

*Research Staff Member, Science and Technology Division, 1801 N. Beauregard Street. Member AIAA.

I. Introduction

THE development of realistic plume flowfield computer models is an ongoing effort of primary importance to the plume community at large. There is, however, a lack of data to validate these models at a level of detail sufficient to elucidate the relevant chemical and thermodynamic processes. The objective of this work is to assess the feasibility of obtaining information on solid plume particle properties using ground-based light detection and ranging (LIDAR) techniques. In relation to this, the interaction of laser radiation with solid aluminum oxide (Al_2O_3) plume particles was examined in order to assess the effectiveness of the LIDAR method as a diagnostic tool. In particular, the possibility of obtaining reasonable estimates of the number density, size distribution, and optical properties of the Al_2O_3 plume constituent through the measurement of scattered intensities was examined.

The general problem of mathematical inversion is nontrivial and has been studied extensively for many years (e.g., Refs. 1–3). The problem of the interaction of radiation with material particles and the retrieval of particle properties from scattered intensities has also received much attention. Established inversion techniques have been applied with varying success in order to obtain estimates of properties of particles existing as atmospheric aerosols in clouds or in plumes (e.g., Refs. 4–8). A rather recent and most notable study of particle sizes in rocket plumes is that of Hermsen[9] in which he originated a method for predicting aluminum oxide particle sizes.

In this paper, we explored some of the possible inversion techniques to retrieve estimates of parameters of interest from the scattered laser signals. The analysis was based on synthesized data that were calculated from known particle size distributions. As yet, no attempt has been made to use experimental data. Thus, we had the advantage of knowing a priori what the correct distribution was. Even though actual field data with associated measurement errors will render the inversion problem more difficult, an initial analysis based on synthesized data can help to identify prospective retrieval methods and to determine, on a first level, what is mathematically feasible when considering the inverse problem.

II. Analysis Procedure

The plumes of solid propellant rockets contain Al_2O_3 in the form of solid particulates whose radius can vary between 0.01–20μ in length, with a mean of 1 ~ 2μ.[10,11] The interaction of these particles with radiation obtainable from a Nd:Glass laser, which has been proposed for an experiment of this type, can then be properly described by the Mie scattering theory.[12] Some wavelengths that are potentially available from a Nd:Glass laser are the fundamental at $\lambda = 1.06\mu$, its harmonics at $\lambda = 0.35\mu$, 0.53μ, and the HD Raman shifted counterpart at 1.7μ. Solid state InGaAs photodiode detectors, which are highly sensitive in the 1.0–1.7μ spectral region, will be used in the measurement of the returned signal.

Our analysis is based on the generalized LIDAR equation[13]:

$$P_r(\nu_r,R) = P_o(\nu_o)KT(\nu_o)T(\nu_r)Y(R)\Delta R\beta(\nu_o,R)A_r/R^2 \quad (1)$$

where the total transmittance $T(\nu)$ can be expressed as

$$T(\nu) = \exp\left[-\int_o^R \alpha(\nu, r)\, dr\right] \quad (2a)$$

with

$$\alpha(\nu,r) = \sigma(\nu)\, N(r) \quad (2b)$$

The scattered laser power received by the detector can be computed from Eq. (1). The values of τ_p (10 ns), τ_c (10 ns), K (0.1), and A_r (5000 cm²) were chosen in accordance with the specifications of the assumed instrumentation. The value of $Y(R)$ was set = 1, corresponding to a total overlap of transmitter and receiver fields of view. A pulse of 300 mJ energy and 10 ns duration is typical for a Nd:Glass laser. In a bistatic arrangement of the laser scattering experiment, the transmitter and receiver are spatially separated, whereas in a monostatic arrangement, they coincide.

The volume scattering coefficient β in Eq. (1) depends on the size distribution of particles and is given by the integral

$$\beta(\lambda,\theta) = N\int_{a_{\min}}^{a_{\max}} f(a)\frac{d\sigma}{d\Omega}(\lambda,\theta)\, da \quad (3)$$

Mie theory gives an exact solution to the problem of absorption and scattering of light from spherical particles of arbitrary radius and refractive index. In special cases of nonspherical geometry, such as ellipsoidal, it can provide a first-order description of the same phenomena. The general case, however, of irregularly shaped scatterers is extremely difficult to treat. For this reason, we began our calculations by assuming spherical particles, even though their exact shape in the rocket plume is uncertain. The other simplifying assumption is that of single as opposed to multiple scattering, which is strictly valid for optically thin media. In optically thick media, the received signal P_r includes photons that have been scattered more than once. Hence, it will exceed the value obtained from Eq. (1). The effects of multiple scattering depend on the size of the scattering particles, the values of the absorption and scattering coefficients α, the time after pulse transmission, etc. In general, a theoretical treatment of multiple scattering is complex and has only in some cases been approximated through involved numerical simulation (e.g., Ref. 14). For the particle sizes and densities obtained from both high- and low-altitude flowfield codes (CHARM[15] and SPF2[16]), our calculations show that optical thinness holds everywhere except perhaps near the nozzle, where concentrations are higher. Therefore, the assumption of single scattering remains valid in this work.

The first step in our calculations was the determination of the differential scattering cross section $d\sigma/d\Omega$ as a function of λ, θ, and the particle radius a. This was done using a modified version of the Mie scattering code of Bohren and Huffman,[12] which gives various scattering parameters for a homogeneous sphere. To calculate $d\sigma/d\Omega$, it is necessary to input the real and imaginary parts of the index of refraction n of the scattering material. For Al_2O_3, this set of data was obtained from an SPF2-SIRRM (Standardized Infra-Red Radiation Model) file,[16,17] which contains a combination of theoretical and experimental values.

In order to investigate the effect of size distribution on the volume coefficient β and the received laser power P_r, several representative models were chosen. Nine different continuous distributions were obtained from the literature[11,18,19] and were of an exponential or log-normal nature. The mode radii varied between 0.01 and 8μ and covered the range from submicron to large particle distributions (Table 1).

A representative discrete size distribution was obtained from the CHARM simulation data file for an altitude of 100 km[15] with radii a = 0.5, 1.0, 2.0, 3.0, and 4.0μ and corresponding densities $N(a)$ = 7, 7, 28, 230, and 56/cm³.

III. Clear Atmosphere Results

Assuming a particle density $N = 10^3$/cm³, the LIDAR equation was used to compute P_r, which was then examined as a function of scattering angle θ, wavelength λ, and range R. Representative plots, corresponding to a possible plume particulate size distribution (model 4 in Table 1) and an atmospheric model with only gas molecules (i.e., no aerosols), are shown in Figs. 1–3. Figure 1 is a plot of P_r vs range for 10 km $< R <$ 100 km and $\theta = 180$ deg. The point of intersection of each curve with the detector sensitivity line for the same wavelength corresponds to the maximum detectable range for that value of λ. The horizontal line in the figure represents the detector sensitivity at $\lambda = 1.7\mu$.

Figure 2 shows the variation of P_r with λ at $R = 100$ km. The low minimum at $\lambda = 0.35\mu$ is caused by the attenuation factor $\exp(-\sigma N_A R)$, in which σ is inversely proportional to λ^4. Thus, the shorter wavelength signals are attenuated most strongly by the atmosphere. The triangular points represent the detector sensitivity for each particular wavelength. It can be seen that the corresponding curves lie mostly above these points. At 100 km detection range and a backscattering angle of 180 deg, three wavelengths would thus be useful for this particular set of parameters.

Figure 3 is a plot of P_r vs θ at $R = 100$ km. The portion of each curve lying below the corresponding detector sensitivity line represents the angular region for which the returned signal is too low to be detected. For 0 deg $< \theta <$ 180 deg, all of the models studied yielded curves of P_r with the same general features as those of Fig. 3: a maximum at 0 deg, a secondary maximum at 180 deg, and a minimum at 120–140 deg. The detailed shapes of P_r vs θ were, however, model dependent. Since the angular dependence of P_r, as well as all of the information on species properties, is contained in the volume scattering coefficient, we focus our attention on β to analyze the results of our calculations.

Table 1 Size distribution models

Model number	a_{mode}, μ	a_m, μ
1	7.0	19.61
9	8.0	16.70
8	4.0	11.02
7	2.0	7.89
5	0.01	6.44
4	0.561	3.48
3	0.198	2.20
6	0.2	1.90
2	0.652	1.21

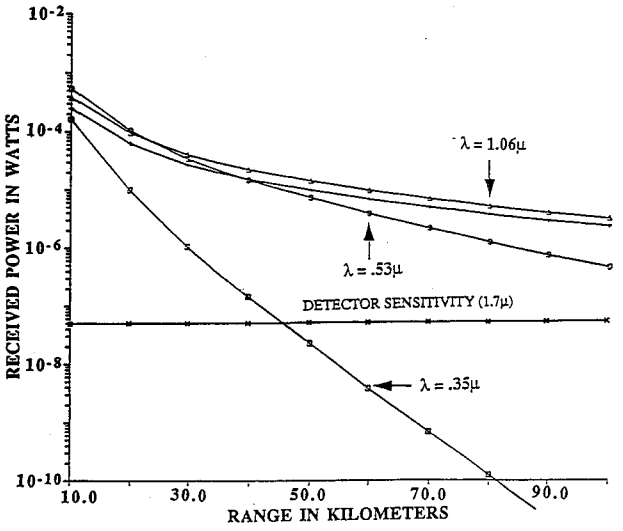

Fig. 1 Received laser power vs range: θ = 180 deg; $N = 10^3$ cm^{-3}; Distribution model 4; clear atmosphere.

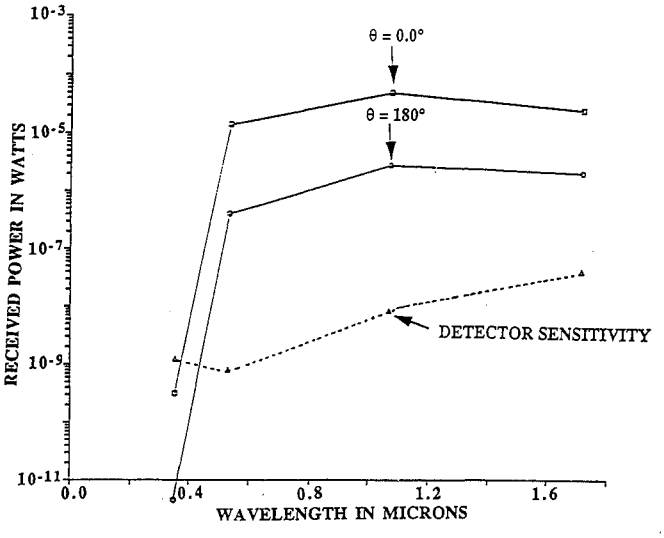

Fig. 2 Received laser power vs wavelength: range = 100.0 km; $N = 10^3$ cm^{-3}; Distribution model 4; clear atmosphere.

IV. Effect of Atmospheric Attenuation

Severe limitations can be imposed on the minimum detectable power by the attenuation of the laser pulse on its way to and from the scattering volume. Atmospheric attenuation is incorporated into the LIDAR equation [Eq. (1)] through the factors $T(\lambda_o)$, $T(\lambda_r)$,

$$T(\lambda) = e^{-\sigma N_A R} \tag{4}$$

where R is the extinction path length, N_A the atmospheric constituent number density, and σ the extinction cross section through both scattering and absorption by gases and particles.

Three situations have been considered so far in this analysis:

1) In order to study in isolation the effects of density N and particle size distribution on the received power, a constant atmospheric transmittance of 0.8 was assumed. For a signal-to-noise (S/N) ratio of 5 and a noise-equivalent power (NEP) of 10^{-8} W, the maximum range corresponding to a detectable signal was obtained by solution of the LIDAR equation for R. In the case of $T(\lambda) = 0.8$, R_{max} is > 200 km at θ = 180 deg for all wavelengths and $N = 1000/\text{cm}^3$.

2) For a clear atmosphere containing only gas molecules whose sizes are small compared to the laser wavelengths, the scattering cross section is given by the Rayleigh theory:

$$\sigma_R = 4.56[\lambda(\mu)/0.55]^{-4} \times 10^{-27} \text{ cm}^2 \tag{5}$$

for altitudes below 100 km.[13] In this case, atmospheric attenuation depends on the wavelength of the transmitted radiation as well as on R. For a sea level density of $N_A = 2.55 \times 10^{19}/\text{cm}^3$ (worst case scenario, since density decreases with altitude), and the same detector sensitivity, the maximum detection ranges for θ = 180 deg varied from 35–58 km for λ = 0.35μ (depending on the model), 105–200 km for λ = 0.53μ, and to over 200 km for λ = 1.06, 1.7μ.

3) For an atmosphere with aerosols or pollutants, an empirical equation[13] was used to calculate the transmittance, which decreases mainly due to absorption:

$$\alpha = (3.91/V_m)\,[0.55/\lambda(\mu)]^q \tag{6a}$$

$$q = 0.585\,[V_m(\text{km})]^{1/3} \quad \text{for} \quad V_m \le 6 \text{ km} \tag{6b}$$

$$q = 1.3 \text{ for "average seeing conditions"} \tag{6c}$$

For visibility $V_m = 16$ km, it was found that aerosols markedly reduced the detectability of the signal. For model 6 and $N = 1000/\text{cm}^3$, the results are shown in Table 2.

The detectability of the signal is a very strong function of atmospheric composition and weather conditions. The previous examples serve mainly to illustrate this variation.

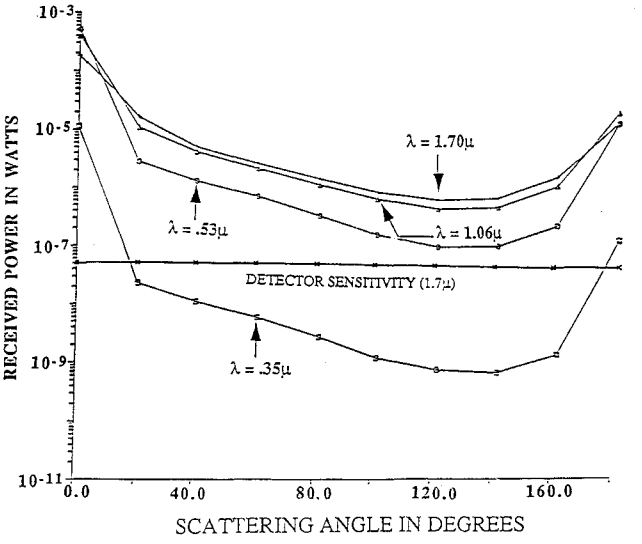

Fig. 3 Received laser power vs scattering angle: range = 40.0 km; $N = 10^3$ cm^{-3}; Distribution model 4; clear atmosphere.

V. Effect of Particle Size

In examining flowfield solutions for high- and especially low-altitude plumes, we found that there is a spatial variation of the particle size distribution function within the range resolution cell ΔR, which for the instrumentation considered in this paper is 3.15 m. Depending on the aspect angle of laser beam and plume axis, this variation can be considerable, es-

Table 2 Maximum detectable ranges for an atmosphere with aerosols

λ, μ	0.35	0.53	1.06	1.7	
R_{max}, km	9	13.50	24.25	34.75	(θ = 180 deg)

pecially near the nozzle where the plume width is smaller than ΔR. The LIDAR measurements considered herein will, therefore, represent an average over the range resolution cell, which becomes more representative of a localized measurement the farther downstream one goes. However, even average estimates of the particulate parameters would prove valuable as a laser diagnostic since they can be compared with corresponding average values predicted by the flowfield simulation codes. For instance, they would be very useful in exploring the variation of the average radial parameters with axial distance, which can be pronounced. With this consideration in mind, we report the results of our analyses of the effect of particle size on the LIDAR signals.

The values of β were found to vary greatly in magnitude for the different models, especially at $\theta = 0$ and 180 deg. However, the magnitude of β alone cannot be used immediately to extract information on the size distribution because β also depends on N, which is unknown. On the other hand, the detailed shapes of the curves of β vs θ and λ or, equivalently, the ratios of β for different angles at constant λ and vice versa are density independent and can yield clues as to the size distribution of the particles producing them. The ratios of the volume scattering coefficients were calculated for all wavelengths at various angles, including 0/180 deg, 0/100 deg, and 180/160 deg. It was seen that they are roughly proportional to the size of the largest particles in the distributions. A measure of this size is the radius a_m for which

$$\int_{0.01}^{a_m} f(a)\, da = 0.985$$

i.e., ~99% of the particles in the distribution have radii smaller than a_m. The values of a_m corresponding to each size distribution model are listed in Table 1. Figure 4 contains plots of $\beta(\lambda, 180\text{ deg})/\beta(\lambda, 160\text{ deg})$ vs a_m for three values of λ. Model 1, which contains large particles, gives the highest values for $\beta(\theta_1)/\beta(\theta_2)$ for all λ, whereas model 2, which describes a submicron particle distribution, gives the lowest ratios. On the other hand, calculation of the average value of the differential cross section

$$\frac{\overline{d\sigma(\lambda,\theta)}}{d\Omega} = \int_{0.01}^{a_{max}} f(a)\, \frac{d\sigma}{d\Omega}(\lambda,\theta)\, da$$

produces a monotonic dependence on a_m, as well.

Examination of the ratios of β at a single angle but two different wavelengths reveals only a slight variation with distribution model, as opposed to the orders of magnitude increase observed for multiangle measurements. For example, the ratio of $\beta(1.06\mu, 180\text{ deg})/\beta(1.7\mu, 180\text{ deg})$ varied only between 1.2 for the largest size particle distribution to 2.9 for the smallest size distribution. It is not certain that such differences could be distinguished experimentally and, hence, exploited in the extraction of useful information regarding particle properties.

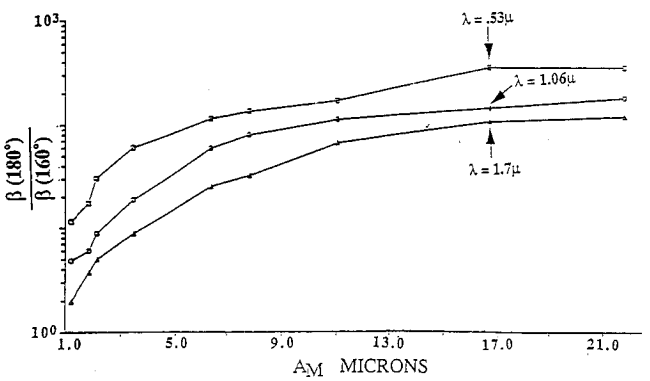

Fig. 4 Ratios of volume backscattering coefficients.

VI. Particle Size Retrieval Methods

A. Bistatic Measurements

The functional dependence of the ratios of β on distribution model suggests a possible method for obtaining estimates of the concentration and sizes of the scattering particles for bistatic arrangements. Measurements at $\theta = 0$ deg would be most useful because of the more pronounced variation of the scattering cross section as well as of the ratios $\beta(0\text{ deg})/\beta(180\text{ deg})$, $\beta(0\text{ deg})/\beta(100\text{ deg})$ in the forward direction. However, this is not possible for a ground-based LIDAR system tracking a moving body. Also, atmospheric attenuation of the laser radiation (Sec. IV), especially in the case of high-altitude rockets, will limit the choice of receiver locations to backward scattering angles close to 180 deg. In the interest of good statistics, it is desirable to collect as much data as possible in any experiment; in this case, values of P_r at several angles and wavelengths. Practical considerations, however, limit the number of receivers that can be set up to at most two. This places the wealth of information inherent in measurements at forward scattering angles out of reach and forces us to focus our attention on angles around 180 deg. It can be seen from Fig. 4 that even in this angular region the proportionality between $\beta(180\text{ deg})/\beta(160\text{ deg})$ and a_m can be exploited in the following way.

First, one would calculate the ratio $P_r(180\text{ deg})/P_r(160\text{ deg})$, which is density independent for a continuous distribution. For a constant wavelength, this ratio is equal to that of the average cross sections at the two angles,

$$S = \frac{\overline{d\sigma(\lambda,180\text{ deg})}}{d\Omega} \Big/ \frac{\overline{d\sigma(\lambda,160\text{ deg})}}{d\Omega}.$$

Interpolation in a theoretically determined curve of S vs a_m can give an estimate of the largest size particles in the distribution. Using this value of a_m, a second interpolation in a curve of $\overline{d\sigma(\lambda,180\text{ deg})}/d\Omega$ will give an estimate of the backscattering cross section weighted over the distribution [the integral in Eq. (3)]. Insertion of this value in the expression for β [Eq. (3)] will immediately yield an estimate of the number density of particles in the scattering volume. As a consistency check, this procedure should be repeated for all available pairs θ_1, θ_2 and for all wavelengths. The final estimates for a_m, $d\sigma/d\Omega$, and N will be given by the averages of the individual estimates.

The ratios $\beta(\lambda,\theta_1)/\beta(\lambda,\theta_2)$ apparently do not depend on the details of the distribution as much as they do on the magnitude of the largest radii that can be expected to occur in the distribution with a reasonable probability. The scattering is therefore dominated by the largest size particles. Models 6 and 2, although different in functional form, give roughly the same values for the ratios of β because of the near equality of a_m for the two cases.

Armed with a preliminary knowledge of N and a_m, one can then proceed to a mathematically more sophisticated method of determining the detailed parameters of the distribution. These we discuss in connection with multiwavelength measurements in the following.

B. Monostatic Measurements

The limitations of the type of ground-based experiment under proposal render it difficult to obtain unambiguous bistatic measurements. For this reason, we focused next on the feasibility of retrieval of plume particles properties from multiwavelength measurements at the single backscattering angle of 180 deg. A monostatic setup would minimize technical problems, as well as uncertainties arising from the nonoverlap of the fields of view of transmitter and receiver. Since the

ratios of β for a monostatic setup do not vary significantly with distribution model, we must resort to more detailed inversion techniques than that used for multiangle measurements. Two of the inversion methods implemented in the present analysis were the following.

1) A modified version of a retrieval method found in the literature[20] that makes use of the Twomey nonlinear iterative inversion scheme[21] to retrieve the unknown size distribution. The author of Ref. 20 applied the method with moderate success to retrieval of size distributions from multiangle measurements. Here, we tried it on multiwavelength measurements.

Following the example of Young,[20] we chose to work with the mass loading distribution $m(a)$, which may be expressed in terms of the number density distribution as

$$m(a) = \frac{4\pi}{3} \rho\, a^3\, n(a) \tag{7}$$

Equation (3) for β then becomes

$$\beta(\lambda, \theta) = \int_{a_{\min}}^{a_{\max}} K(\lambda, \theta, a)\, m(a)\, da \tag{8a}$$

where

$$K(\lambda, \theta, a) = \frac{3}{4\pi\rho} \frac{1}{a^3} \frac{d\sigma}{d\Omega}(\lambda, \theta) \tag{8b}$$

$K(\lambda, \theta, a)$ is called the kernel function and is a weighting factor for the contribution to $\beta(\lambda, \theta)$ of particles with radii between a and $a + da$. As stated in Ref. 20, the functional form of $K(\lambda, \theta, a)$ determines the feasibility of performing an inversion and the accuracy with which it can be performed. The kernel for this problem is shown in Fig. 5 as a function of the dimensionless size parameter $x = 2\pi a/\lambda$ and for $\theta = 180$ deg. The kernels $K(\lambda, \theta, x)$ essentially limit the size parameter range over which an inversion can be effected. The kernel of Fig. 5 is appreciably different from zero between $x \cong 0.5$ and 200. Outside this region, $m(x)$ makes no contribution to $\beta(\lambda, \theta)$ because $K(\lambda, \theta, x)$ is negligible. Using the half-width as a conservative estimate, one can predict a retrieval range between $x \cong 3$–60. If the size distribution is expected to be wider than this, one can move the kernel window across the distribution by varying the wavelength. While the x window remains fixed, the a window varies directly with λ. Thus, for $\lambda = 0.35\mu$, the a window is $a = 0.17$–3.34μ, whereas for $\lambda = 1.7\mu$, it is $a = 0.81$–16.23μ. Since particle distributions with radii <0.17 and $>16\mu$ are highly unlikely in plumes, this will adequately cover the size ranges that are expected.

A second feature of the kernel is its rapid oscillatory behavior, which has consequences on the accuracy of the inversion method itself. The Twomey nonlinear algorithm is set forth in Ref. 20 and is shown as a computational flowchart there. One begins with the known measurements of $\beta_i(\lambda_i, \theta)$ for $\theta = 180$ deg and $\lambda_i = 0.35, 0.53, 1.06, 1.7\mu$, the calculated kernel function $K(\lambda, \theta, a)$, the maximum over a of the kernel functions $K_{\max}$, and a first guess solution $m_1(a)$. The value β_i obtained from the guess solution is then used along with the observed β to compute a correction parameter ξ. This parameter is then combined with the normalized kernel $K/K_{\max}$ to modify the first guess solution. The loop is continued over all available wavelengths λ_i. The end result is one cycle of the iteration process. The value of $m(a)$ obtained from the first cycle is subsequently used as an initial guess going into the second cycle. The process is continued until some predefined convergence criterion is met.

In order to try out the Twomey inversion algorithm, a test case was established using model 6 (Table 1) of our study, $n(a) = 6493.8\, a^{\cdot 6} e^{-3a}$, as the true size distribution with the particle number density $N = 1000/\text{cm}^3$. Transforming to the mass loading distribution and integrating over the corresponding range of radii we get

$$6493.8 \times \frac{4\pi}{3} \times 3.7 \int_{0.01}^{2} a^{3.6} e^{-3a}\, da = 8.58 \times 10^{-9}\ \text{g/cm}^3 \tag{9}$$

for the mass density of particles. The algorithm was tested for three different initial guess solutions. Convergence was set at the number of iterations for which $\beta\text{OBS}/\beta\text{CAL} = 1 \pm 5 \times 10^{-4}$. The first guess solution was $n(a) = 7200a^2 e^{-2.4\, a^3}$ with a mass loading $= 8.00 \times 10^{-9}$ g/cm³. The retrieved mass distribution is shown as curve 2 in Fig. 6. The degree of fluctuation is disconcerting and arises from the nature of the kernel function. Following Ref. 20, we tried to suppress the fluctuations by explicit smoothing of the form:

$$\overline{m}(j) = \frac{1}{2MS + 1} \sum_{j-MS}^{j+MS} m(k) \tag{10}$$

with $MS = 3$. The degree of fluctuation is thus reduced (curve 3 of Fig. 6), but overall agreement between retrieved and true distributions is still not very good. As a way of improving the accuracy of the results, the author of Ref. 20 applied a modified inversion scheme, consisting of many cycles of iteration similar to the one described earlier, but in which the smoothed version of the end result of one cycle is used as an initial guess in the next cycle. This in effect amounts to a superiteration. In the present case, the result of 15 cycles of superiteration is shown in Fig. 7, along with the true distribution and with the initial guess. No significant improvement was achieved beyond 15 cycles. For this particular initial guess, the center of the distribution was retrieved with considerable accuracy. Agreement was closer over the short radius wing of the distribution, most likely a result of the choice of initial guess solution, which is a small particle distribution.

It is not difficult to see that the accuracy of the retrieved distribution will depend on the initial guess. The closer this is to the true distribution, the better will be the result. In reality, the nature of the particle size distribution is unknown in the absence of auxiliary measurements. Such being the case, a most general, unbiased initial guess might be a distribution

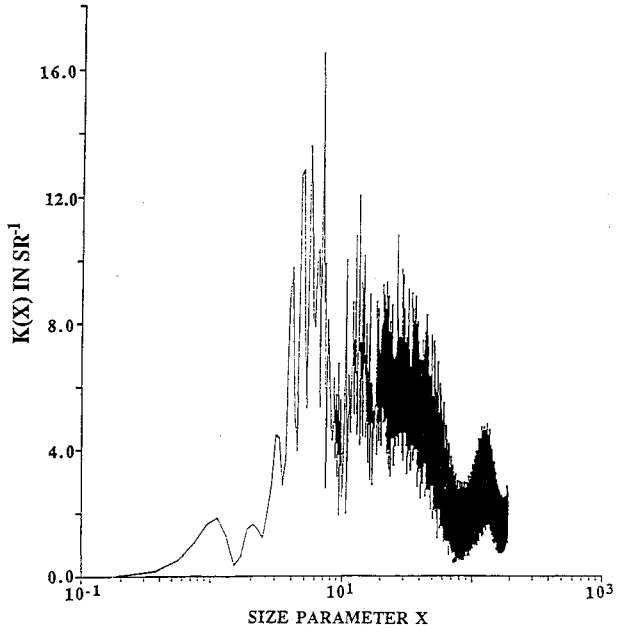

Fig. 5 Kernel in defining integral of the volume backscattering coefficient.

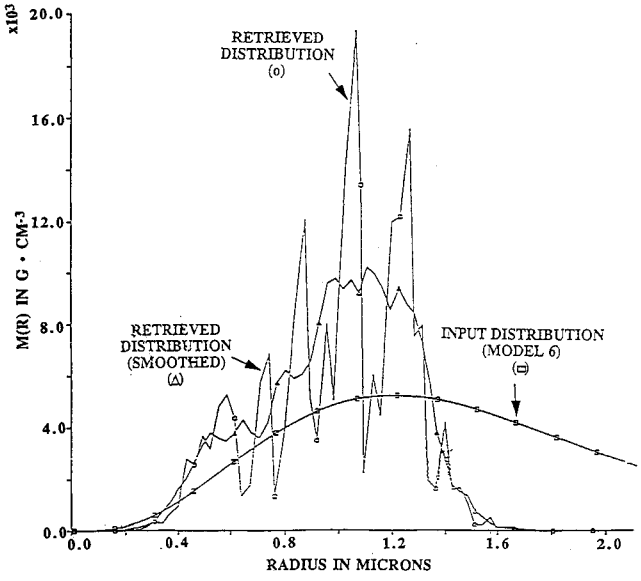

Fig. 6 Retrieved functions resulting from one iteration of the Twomey nonlinear method.

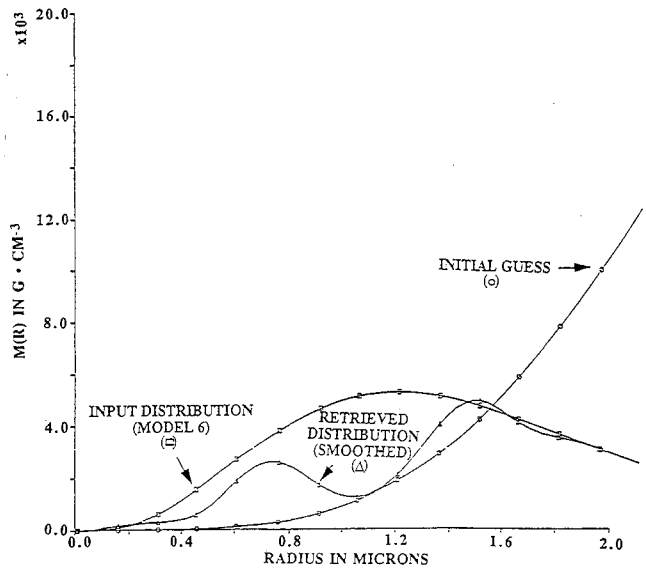

Fig. 8 Retrieved functions resulting from multiple iterations of the Twomey method, initial guess 2.

that is constant within some range of radii. The result of such an initial guess, with a mass loading of $\approx 8.4 \times 10^{-9}$ g/cm^3 over a radius range of 0.01–3μ is presented in Fig. 8. Overall agreement is not bad as far as the order of magnitude predictions are concerned. However, retrieved and true distributions again do not agree in detail. A third initial guess, $n(a) = 500\, a^2 e^{-a}$, a large particle distribution (mode radius = 2μ) produced results similar to those of Fig. 8.

The fact that all of these retrieved distributions yielded values of β that agree with the observed values to within five parts in 10^4 implies that each one of them is "correct" and equally probable as far as producing the given data, even though they did not in detail agree with the true distribution. Implementation of the Twomey nonlinear inversion method, in this case, has shown that one cannot unambiguously determine the actual particle size distribution from multiwavelength, monostatic measurements. Rather, it might be possible to retrieve one of many probable size distributions, which will depend on the initial guess, the smoothing constraint and other boundary conditions.

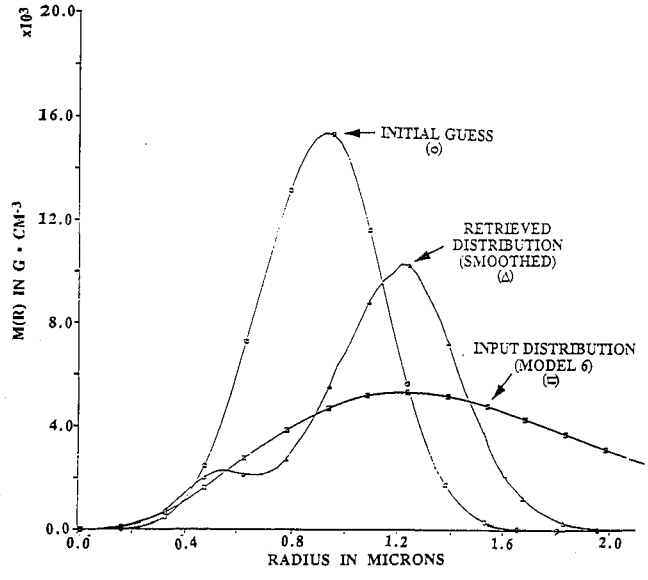

Fig. 7 Retrieved functions resulting from multiple iterations of the Twomey method, initial guess 1.

2) In order to determine exactly how many different types of distribution models will yield essentially the same values of β_i, we applied a brute force method of directly fitting a chosen form of distribution to the measured data. In such an approach, one essentially allows the distribution parameters to vary in some systematic fashion until the calculated values of the ratios of β agree with the true values to within a preset tolerance.

Proceeding in such a fashion, we assumed a form $f(a) = Da^b e^{-\alpha a}$, based on which we calculated the ratios of β_i for $\theta = 180$ deg and the four values of λ. D is a normalization constant equal to $b!/\alpha^{b+1}$. The parameters α, b were incremented sequentially in steps of 0.1, whereas $a_{\max}$ increased in steps of 1μ. Those combinations of parameters that yielded ratios to within 3% of the true ratios were printed out. Results of calculations using models 6, 3, and 7 of our study showed that such an approach will yield accurate estimates for the maximum size radius in the distribution and an estimate for the mode radius anywhere between 0.5–2 times the true value. An estimate for the particle number density can be obtained from the distribution parameters by evaluation of the integral

$$\int_{0.01}^{a_{\max}} \frac{d\sigma}{d\Omega} f(a)\, da$$

and substitution into the equation for β [Eq. (3)].

C. Bistatic or Monostatic Measurements (Discrete Distribution)

The discrete distribution gave results for β and P_r with general features similar to those of the continuous distributions. The attempt at a linear inversion in this case is a first step in the implementation of a more complex scheme, with the purpose of establishing the existence of at least one solution to the parameter retrieval problem. We emphasize the fact that the results reported here were obtained using perfect (noise-free) data. In addition to the question of existence, there are also the questions of uniqueness and stability, which must be explored in a complete solution of the inverse problem. With this caveat, we proceed to describe the linear inversion routine used on the discrete distribution. First, the interval $[0, a_m]$ (a_m is the estimate for the maximum radius, which can be gotten as described earlier) is subdivided into small bins of length da_i ($i = 1, N$) and a corresponding number of radii a_i are selected, one in each bin. The number of bins N should equal the number of available data points (values

of β for various λ and θ). We then proceed to set up a system of N linear equations

$$\sum_i \frac{d\sigma(\lambda,\theta,a_i)}{d\Omega} f(a_i) = \beta(\lambda,\theta)$$

with the number densities $f(a_i)$ corresponding to each a_i as unknowns. In order to get a unique solution set, the number of unknowns $\beta(a_i)$ must equal the number of data points $\beta(\lambda_i,\theta_i)$. Therefore, the more data available, the better the chances of arriving at an accurate solution for the discrete number densities and the corresponding radii. Difficulties associated with numerical problems (such as singularity of matrices) must be carefully dealt with.

In our test case, a 6×6 linear system was set up for six unknowns and solved using an International Mathematical and Statistical Libraries (IMSL) routine based on Gaussian elimination. There appeared to be only one set $\{a_i\}$ that gave a physical solution for $f(a_i)$, most likely due to the nature of the functional dependence of $d\sigma/d\Omega$ on a. Any other combination of radii gives unphysical results [negative numbers for $f(a_i)$]. The method then consists in trying all combinations of a_i, one in each bin, in increments as small as one chooses. In the test example, we proceeded in steps of 0.1μ for a_i in the intervals [0,1], [1,2], [2,3], [3,4], [4,5] and obtained a unique solution for the set a_i, $f(a_i)$, which agreed with the true values to within 0.3%. The use of actual field data will, however, complicate the implementation of this method and may partially alter the results.

VII. Conclusions

The analysis of laser scattering by Al_2O_3 particulates in a plume volume has shown, based on the use of synthesized data, the following:

1) The detectability of the returned signal is a strong function of atmospheric conditions. The maximum detectable range will also depend on the laser wavelength, the concentration and optical properties of the scattering particles, as well as the detector sensitivity.

2) From bistatic measurements, one may retrieve estimates of the largest size scattering particles and particle concentrations from the ratios of the measured values of the returned power. It was found that the volume scattering coefficients do not depend as much on the detailed parameters of the size distribution, but on the magnitude of the largest size particles, which, therefore, dominate the scattering.

3) In the case of monostatic measurements, one must resort to more sophisticated inversion techniques in order to retrieve plume particle properties. Implementation of the Twomey method showed that the retrieved solution will not be unique. Direct fitting of data to a parametrized distribution form produced an accurate estimate of the maximum particle radius while it gave the possible range of other distribution parameters, such as mode radius. Each method has its merits. Therefore, we believe that application of both would provide useful information.

References

[1]Lavrientev, M. M., *Some Improperly Posed Problems of Mathematical Physics*, Springer-Verlag, Heidelberg, Germany, 1967.

[2]Sabatier, P. C., *Proceedings of the Royal Society of London*, 1974, p. 49.

[3]Tikhonov, A. N., and Goncharsky, A. V., *III-Posed Problems in the Natural Sciences*, MIR Publishers, Moscow, Russia, 1987.

[4]Twomey, S., "Information Content in Remote Sensing," *Applied Optics*, Vol. 13, No. 4, 1974, p. 942.

[5]Chow, L. C., and Tien, C. L., "Inversion Techniques for Determining the Droplet Size Distribution in Clouds: Numerical Experiments," *Applied Optics*, Vol. 15, Feb. 1976, p. 378.

[6]Curry, B. P., Kiech, E. L., and Jones, J. H., "Two Particle Size Inversion Procedures for Interpretation of Scattering Measurements," Arnold Engineering Development Center, TR-83-32, Arnold AFS, TN, Nov. 1983.

[7]Herman, B. M., Browning, S. R., and Reagan, J. A., "Determination of Aerosol Size Distributions from Lidar Measurements," *Journal of the Atmospheric Sciences*, Vol. 28, No. 5, 1971, p. 763.

[8]Davis, P. A., "The Analysis of Lidar Signatures of Cirrus Clouds," *J. of Applied Optics*, Vol. 8, 1969, p. 2099.

[9]Hermsen, R. W., "Aluminum Oxide Particle Size for Solid Rocket Motor Performance Prediction," *Journal of Spacecraft*, Vol. 18, No. 6, 1981, p. 483.

[10]Brown, B., and McArty, K. P., *8th International Symposium on Combustion*, Williams & Wilkins, Baltimore, MD, 1962, p. 814.

[11]Bauer, E., and Carlson, D. J., "Mie Scattering Calculations for Micron Size Alumina and Magnesia Spheres," *Journal of Quantitative Spectroscopy and Radiative Transfer*, Vol. 4, 1964, p. 363–374.

[12]Bohren, C. F., and Huffman, D. R., *Absorption and Scattering of Light By Small Particles*, Wiley, New York, 1983.

[13]Collis, R. T. H., and Russell, P. B., "LIDAR Measurement of Particles and Gasses by Elastic Backscattering and Differential Absorption," Hinkley, E. D. (ed.), "Laser Monitoring of the Atmosphere," *Topics in Applied Physics*, Vol. 14, Springer-Verlag, New York, 1976.

[14]Plass, G., and Kattawar, G., *Applied Optics*, Vol. 10, 1972, p. 2304.

[15]Smith, C. E., "The Composite High Altitude Radiation Model (CHARM)," *17th JANNAF Exhaust Plume Technology Meeting*, CPIA Vol. 1, 1988, p. 53.

[16]Dash, S. M., Pergament, H. S., and Thorpe, R. D., "The JANNAF Standard Plume Flowfield Model (SPF2)," 11th JANNAF Plume Technology Meeting, CPIA Vol. 1, p. 345, 1979. "The JANNAF Standard Plume Flowfield Model (SPF/2)," Vols. I and II(U), Science Applications, Inc. Preprint; SAI/PR TR-18, May 1989.

[17]Ludwig, C. B., Malkmus, W., Freeman, G. N., Slack, M. W., and Reed, R. A., "A Theoretical Model for Absorbing, Emitting and Scattering Plume Radiation," *Progress in Astronautics and Aeronautics: Spacecraft Radiative Transfer and Temperature Control*, Vol. 83, edited by T. E. Horton, AIAA, New York, 1982, p. 111.

[18]Fenn, R. W., et al., "Optical and Infrared Properties of the Atmosphere," Jursa, A. S. (ed.), *Handbook of Geophysics and the Environment*, Air Force Geophysics Laboratory, 1985.

[19]Bair, C. H., and Allario, F., "Analysis of Differential Absorption LIDAR Technique for Measurements of Anhydrous Hydrogen Chloride from Solid Rocket Motors Using a Deuterium Fluoride Laser," NASA Technical Note D-8390, Langley Research Center, May 1977.

[20]Young, S. J., "Considerations on the Retrieval of Plume Particle Properties from the AFRPL Transmisso-Meter and Polarization-Scattering Experiments," Defense Technical Information Center, Air Force Rocket Propulsion Center, TR-84-047, Edwards AFB, CA, Aug. 1984.

[21]Twomey, S., *Introduction to the Mathematics of Inversion in Remote Sensing and Indirect Measurements*, Elsevier, New York, 1977.